Journal Name

Journal of Materials Chemistry C

Dynamic Article Links▶

ARTICLE TYPE

Characterization of Bimetallic Core-Shell Nanorings Synthesized via Ascorbic Acid Controlled Galvanic Displacement followed by Epitaxial Growth

Tanmay Ghosh, Biswarup Satpati* and Dulal Senapati

This paper describes the role of ascorbic acid in synthesizing bimetallic core-shell nanorings at room temperature. Using two-dimensional (2D) triangular silver nanoparticles as templates we first synthesized 2D triangular gold (Au) nanorings via galvanic replacement reaction and then overgrown Ag on Au
10 nanorings via epitaxial growth process. Transmission Electron Microscopy (TEM) and associated techniques were used for in-depth characterization. TEM study reveals that single crystalline Ag nanoparticles led to the formation of continuous Au nanorings with single crystalline walls and the voids spaces which corroborate with the template shapes only when ascorbic acid was added to growth solution. Both the silver nanoplates and gold nanorings are having (111) planes as the basal planes. Subsequently
15 we have synthesized Au-core — Ag-shell nanorings using previously synthesized Au nanorings as template. Energy dispersive X-ray (EDX) line profile spectra and imaging along with high-angle annular dark field scanning/ transmission electron microscopy (STEM-HAADF) techniques were used extensively for compositional study in addition to energy filtered TEM (EFTEM) imaging.

Introduction

20 In recent years there is a tremendous progress in the design and study of nanomaterials boost up towards biomedical and plasmonic applications, most notable among these being the noble metal nanoparticles. Compared with other nanoparticles metallic nanoparticles has become the subject of extensive
25 research owing to the synthetic control of their size, shape, composition, structure, assembly and encapsulations, as well as theoretical understanding of their properties. Control over the shape, size, composition, and surrounding medium of the metallic nanostructures, in particular anisotropic two-dimensional
30 nanostructures such as nanoprisms, nanodisks, and nanorings, provides effective strategies for tuning the optical, electronic, magnetic, optoelectronic, and catalytic properties distinct from bulk metal.[1-3] Nanorings, the nanostructures with hollow interiors, can be used as extremely small containers for
35 encapsulation which has been extensively explored in applications related to drug delivery,[4] catalysis[5], and protection of environment-sensitive materials such as enzymes.[6] Besides these, noble metal nanorings exhibit plasmonic properties completely different from that of solid nanoparticles made of same material.
40 The electric fields are strongly enhanced over the entire ring surface in case of a nanoring, whereas only small portions or selected areas of the solid plate surface show strong enhancements.[7,8] Control over morphology and void size, noble metal nanorings are useful in fabrication of plasmonic devices
45 and colorimetric sensors, and as near-field absorbers to control

the releasing of drug molecules in a polymer matrix.[9,10]Bimetallic nanoparticles composed of two different metallic elements are of immense concern than its monometallic counterpart, for the improvement of the catalytic properties of metal particles.[11]
50 Although significant efforts have been put forward to the field of nanomaterials synthesis, strong controversy still exist related to the growth mechanisms and the parameters which direct the final size and shape of the nanoparticles.[12-20] Proper understanding of such mechanisms is necessary to carry out the nanoparticle
55 synthesis in a predictable manner.[21,22] In our previous work, we have successfully demonstrated the direct experimental evidence in support of the "silver halide" model proposed by Sigmund et al. to explain the growth mechanism dependable for the formation of different anisotropic particles in nanoparticle synthesis.[3,23]
60 Despite the significant amount of work has already been carried out on noble metal nanoring synthesis following different synthetic methods like: photo-induced process,[24] thermal process,[25]sonochemical process,[26] little has been done following the solution method at room temperature.[27] In this article we will
65 present the room temperature synthesis of Au-core and Ag-shell nanorings and in-depth characterization in every step starting from seed to the final product.
Analyzing the bright-field (BF) TEM, high-resolution TEM (HRTEM) images and selected area electron diffraction (SAED)
70 patterns of these triangular and hexagonal nanostructures, we noticed the formation of well-defined void spaces and highly crystalline walls in these nanorings. These observations also support the epitaxial relationship between the silver nanoplates and gold nanorings for a particular shape (triangular or

hexagonal). TEM related techniques, such as EDX, STEM-HAADF, and EFTEM allowed us to successfully demonstrate the two dimensional nature of the silver nanoplates and Au nanorings and to show that nano-templates and nanorings are made of only silver and gold, respectively.

EXPERIMENTAL SECTION

Chemicals

All the chemicals like Tetrachloroauric acid (HAuCl$_4$, 3H$_2$O; 99.9%, metal basis), Sodium citrate (C$_6$H$_5$O$_7$Na$_3$.2H$_2$O; ACS reagent, 99.0%), Silver nitrate (AgNO$_3$; 99.99%, trace metal basis), Ascorbic acid (BioXtra, 99.0%), Polyvinyle-pyrolidone (PVP, average molecular weight 40000 g mol^{-1}), were purchased from Sigma Aldrich and used as received. For all the preparation steps we have used Milli-Q water with resistivity 18.2 MΩ-cm.

Preparation of Ag NanoPrisms (SNPrs)

In the first step of the synthesis, we prepared a growth solution by mixing 50mL of 0.1mM freshly prepared silver nitrate, 3mL of 30mM sodium citrate, 3mL of 0.5mM,polyvinyle-pyrolidone (PVP) and 250 µL of 30 wt% hydrogen peroxide. The growth solution was stirred vigorously at room temperature for 1.5 minutes. During this stirring process sodium borohydride (100 mM, 100 µL) was rapidly injected to the growth solution and immediately the solution turned into pale yellow, indicates the formation of silver nano seed in the solution which became color less after 30 seconds. After 3 minutes blue colour appeared from the top of the solution and propagates to the bottom of beaker. Finally the solution became completely blue after 20 minutes. The blue colour of the solution indicates the formation of the silver nanoprism. To remove unreacted PVP surfactant, the prepared nanoprism solution was diluted by Milli-Q water and centrifuged three times at 10000 rpm for 30 minutes. For TEM characterization one drop of this solution was put on a carbon coated cupper grid and the water was evaporated to dry the grid properly.[28]

Preparation of Au NanoRings (GNRs)

For the preparation of Au nanorings, Ag nanoprism solution was used as seed solution. In a typical synthesis, ascorbic acid solution (0.1 M, 1.5 mL) was added to the blue coloured Ag nanoprism solution (20 mL) followed by the addition of tetrachloroauric acid (0.1 M, 100 µL). The solution becomes grey indicating the formation of different anisotropic Au nanorings. In the synthesis process the replaced silver atoms become AgCl which precipitate out from the solution and was removed by using ammonium hydroxide solution. Leached out PVP surfactant from SNPrs was removed by the addition of Milli-Q water to this grey coloured solution and subsequent centrifugation of the mixture for a period of 20 minutes at speed of 5000 rpm. This process was repeated for two times. The resultant GNR solution was then drop casted to a 300 mesh carbon coated cupper grid for TEM study.[29] To investigate the role of ascorbic acid in the GNR formation we have prepared GNRs without ascorbic acid where 30 µL tetrachloroauric acid was added to 5 mL of SNP solution. Keeping the amount of SNP and tetrachloroauric acid solutions fixed, we have prepared GNRs at two different concentrations (100 µL and 300 µL) of 0.1M ascorbic acid.

Preparation of Bimetallic Nano Rings (BiMNRs)

To this as prepared GNR solution (5 mL) we have added AgNO$_3$ (20mM, 500µL) and NaOH (1M, 500µL) solutions one after another which finally produced brown coloured solution containing Au-Ag bimetallic nanoring-like structures. After well centrifugation at a speed of 5000 rpm the sample was made ready for TEM study.

TEM Characterization

All transmission electron microscopy (TEM) investigations were carried out using a FEI, TECNAI G^2 F30, S-TWIN microscope operating at 300 kV. TEM machine is equipped with an Orius CCD camera from Gatan Inc., a HAADF detector from Fischione (Model 3000), an EDS detector from EDAX Inc., and a post-column Imaging Filter (Quantum SE, Model 963) from Gatan Inc.

RESULTS AND DISCUSSION

Optical Properties

The optical properties of metal nanoparticles are determined by their localized surface plasmon resonance (LSPR), the resonance between the collective oscillations of free outer shell electrons of the nanoparticles with the alternating electric field of the electromagnetic radiation.[30] LSPR depends on the dielectric constants of the metal particles and the environment since the surface plasmon resonance frequency; ω_{sp} is related to the dielectric constants ε_1 and ε_2 of the metal and the environment respectively as $\omega_{sp} = \omega_p / \sqrt{\varepsilon_1 + \varepsilon_2}$ where ω_p is the volume plasmon frequency which is determined by electron density of the metal. LSPR also depends on the shape and size of the nanoparticles. Absorption occurs in resonance condition and most notably for gold and silver nanoparticles such resonances usually take place in the visible spectral region.
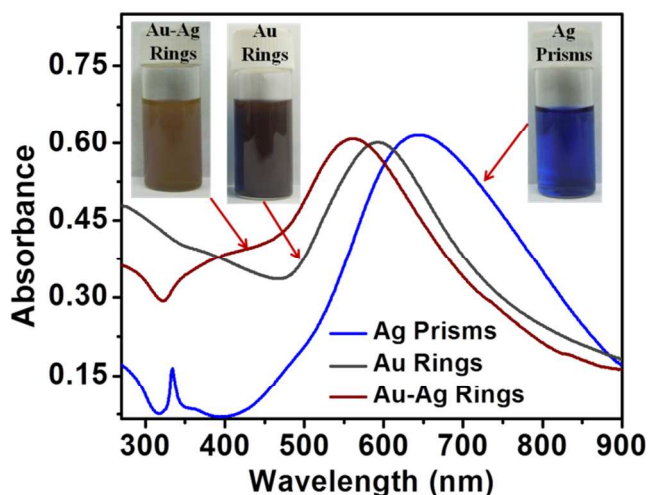

Fig. 1. UV-visible absorption spectra of colloids containing Ag nanoprisms, Au nanorings and Au-Ag bimetallic nanorings. In inset, photographs showing the colours of the colloids of Ag nanoprisms (blue), Au nanorings (grey) and Au core-Ag shell nanorings (brown) in water.

Due to the change in shape, size and types of metal, the resonance condition changes and alters the colour of the nanoparticle dispersion. Because of this, dispersion of Ag nanoprisms within water appeared as blue and that of Au nanorings as grey and Au-

Ag core-shell nanoring as brown. It may be noted that besides the change in colour there is a peak shift of the corresponding UV-visible spectra for two different metallic nanoparticles (Au and Ag) and bimetallic (Au-Ag core-shell) nanoparticles dispersed in water. Figure 1 shows the UV-visible spectra of colloids containing triangular Ag nanoplates (blue line), Au nanorings (grey line) and Au-core—Ag-shell nanorings (brown line). SNPrs exhibit a peak around 645 nm, the peak is shifted to 590 nm after the formation of GNRs and further shifted to 560 nm after the formation of Au-Ag BiMNRs in UV-vis spectral region. One may note that such (UV-vis) investigations can be found in the literature[23] for the Ag nanoplates and Au nanorings synthesized at higher (100ºC) temperature but in our case GNRs and Au-core—Ag-shell BiMNRs were prepared at room temperature. There is a small absorption peak in the short UV range (~330 nm) for SNPr, indicating the presence of small silver nanoparticles as well.[31, 32]

Characterization of Ag Nano Prisms (SNPrs)

The bright-field TEM image of as-prepared silver nanoplates with an average size (edge length) of 50 ± 20 nm is shown in Figure 2a. Figure 2b is the HRTEM image of the as-prepared nanoplates, and the measured fringe spacing is 2.5 Å, which corresponds well with the spacing between 3× (422) planes of the fcc silver

(2.50Å) and this is consistent with the appearance of 1/3{422} type faints spots within the brighter (220) spots in SAED pattern (inset of Figure 2b). Another measured lattice spacing of 1.4 Å in the HRTEM image again corresponds well with the spacing between (220) planes of the fcc silver (1.44 Å). The [111] zone-axis SAED pattern (inset of Figure 2b) exhibits a set of six brighter spots having 6-fold symmetry, which could be indexed to {220} Bragg reflections with a lattice spacing of 1.44 Å, of an fcc single-crystal with a (111) lattice plane as the basal plane. The SAED pattern indicates that the as-prepared nanoplates are single crystals. The flat surface of the silver nanoplate is parallel to the (111) plane as suggested in previous literature.[23] In the SAED pattern, there exist another set of faint spots with hexagonal symmetry within the brighter {220} spots which are indexed as 1/3{422} reflections with a lattice spacing of 2.50 Å, indicating the presence of the single twining boundary within the {111} planes. For single-crystal fcc metal these spots are forbidden but they can appear when there are two twin planes parallel to one another. The appearance of the forbidden 1/3 {422} reflection is often observed on silver or gold nanostructures in the form of thin plates or films bound by atomically flat top and bottom faces.
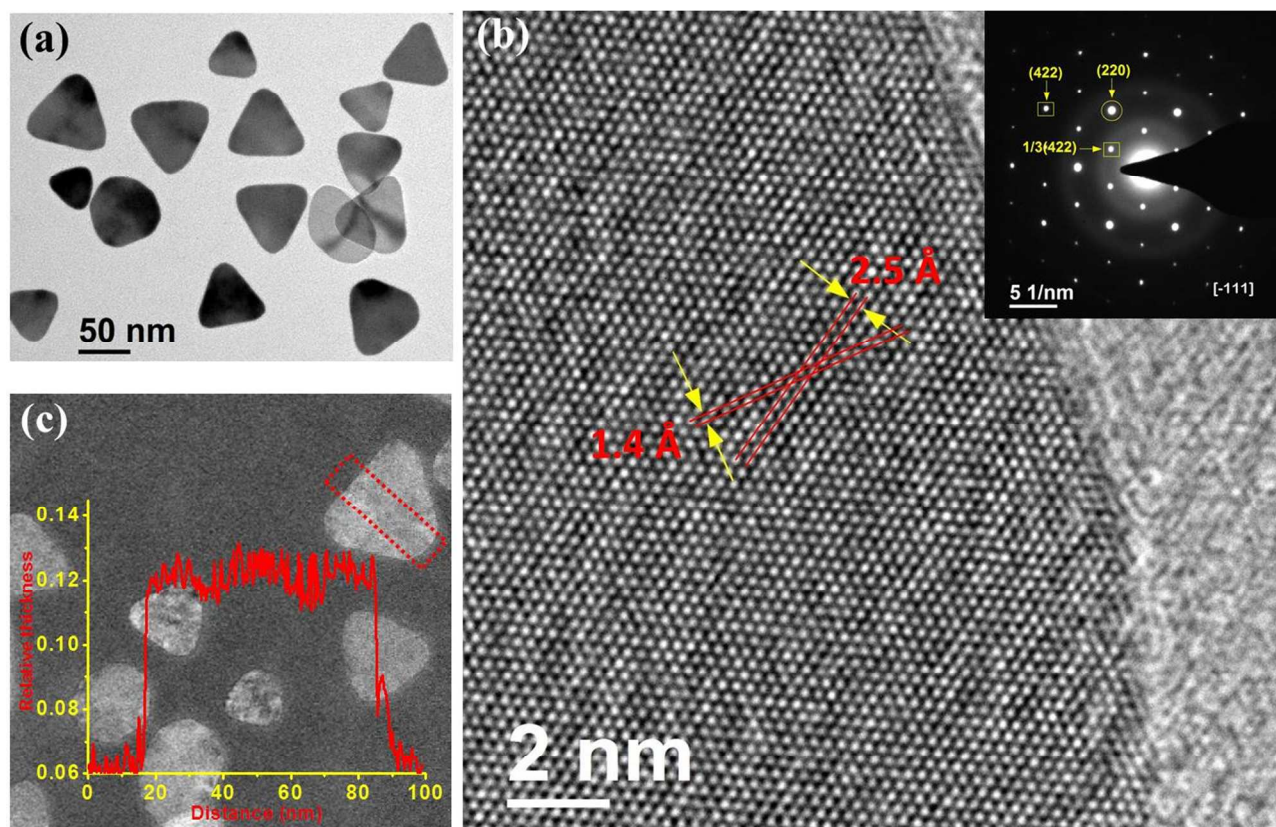

Fig. 2 (a) Bright-field TEM image of Ag triangular nanoplates. (b) HRTEM image from a single a nanoprism. In the inset transmission electron diffraction (TED) of an individual silver nanoplate. The diffraction pattern is characteristic of the [111] zone-axis pattern where nanoplate is lying flat on the substrate with its triangular faces perpendicular to the electron beam. The six intense spots are allowed {220} Bragg reflections (e.g., circled spot, corresponding to the lattice spacing of 1.4 Å), and the six sharp weak spots are indexed as 1/3{422} (e.g., boxed spot, corresponding to the lattice spacing of 2.5 Å). (c) Relative thickness map of the triangular nanoplates. In the inset, graph is the line profile of relative thickness along the dotted box showing flat-top morphology.

The thickness of these nanoplates was measured using log-ratio method. Figure 2c shows the relative thickness (thickness/mean free path) map of these SNPrs acquired using EFTEM mode. The red graph represents the line profile of relative thickness for dotted area over one nanoplate and the measured relative thickness is around 0.05. The inelastic mean free path for silver is

about 145 nm,[33] which gives the absolute thickness of these nanoprisms is around 7 nm. Both the relative thickness map and corresponding line profile indicates two dimensional growths.

Triangular Au Rings and the Role of Ascorbic Acid in Growth Mechanism

The bright-field TEM image of as-prepared silver nanoplates as shown in Figure 2a are used as template for the formation of GNRs.
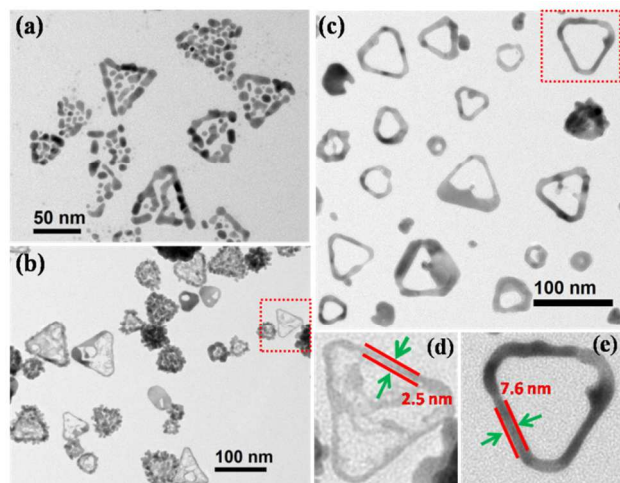

Fig. 3. Ascorbic acid induced structural changes of SNPrs by the addition of 0.1M of 100µL HAuCl$_4$ in presence of (a) 0µL of ascorbic acid, (b) 100 µL of ascorbic acid, and (c) 300 µL of ascorbic acid, (d) and (e) Enlarged images of single GNR, indicated in blue boxes in (b), (c) respectively.

We have prepared GNR structures with and without using the ascorbic acid to study the role of ascorbic acid in growth mechanism as presented in Figure 3a-c. In the absence of ascorbic acid, well defined SNPrs transformed into differentially leached structures (Figure 3a) are made up of small gold nanoparticles and these cannot be considered as well-defined ring structures. Discrete nanoparticles are maintaining the shape of the template. Figure 3b displays the nanostructures prepared by the addition of 100 µL of ascorbic acid in 5 mL of SNPr solution. These structures have well defined wall architecture but the central silver atoms were not fully replaced by gold atoms. So we can consider these as the intermediate structures between SNPr and GNR. Finally we have prepared well defined ring structures by the addition of 300 µL of ascorbic acid in 5 mL of SNPr solution. There are reports in the literature where these kind of well-defined GNR structures were only obtained at higher temperature[25] or under ultrasound irradiation[26]. But in our case we have obtained similar structures at room temperature with addition of ascorbic acid. Here the amount of ascorbic acid is the controlling factor for the formation of well-defined GNR structures from SNPr templates. To the best of our knowledge there is no such report in the literature where the role of ascorbic acid was addressed. We will now discuss the possible scenario behind the formation of GNRs in presence of ascorbic acid. In the absence of ascorbic acid the solution contains only Au^{3+} ions which have strong etching power due to the large difference in reduction potential between gold and silver[25] with $E_{Ag^+/Ag}^{Red} = 0.8V$ vs SHE and $E_{Au^{3+}/Au}^{Red} = 1.5V$ vs standard hydrogen electrode,

SHE allows gold ions to oxidize siver atoms to silver ions and solubilise the SNPrs by a nano-Galvanic cell reaction[27]. Released silver atoms from SNPrs react with the counter ion Cl$^-$ from HAuCl$_4$ and precipitates out as AgCl from the solution. On the course of the etching process PVP also released out from the SNPrs along with silver atoms acts as active surfactant to form gold nano particles. According to the literature, the free energies associated with the crystallographic planes of an fcc metal increases in the order: $\gamma_{(111)} < \gamma_{(100)} < \gamma_{(110)}$[34]. For thin SNPrs, atomically flat top and bottom faces are with [111] facets and the edges are with [110] facets. In absence of ascorbic acid, system doesn't generate any preformed gold nanoparticles[35] for gold plating to form GNRs. So, absence of ascorbic acid leads the Au^{3+} ions primarily to leach the SNPrs first to release both Ag+ ions and the associated PVP surfactants which then act as surfactant to form gold nanoparticles. In absence of preformed GNPs [110] facets leaches first due to its highest free energy or least stabilization energy. Since [111] crystal planes (top and bottom) are atomically flat and lower in surface energy compared to faceted edges [110], subsequent gold plating on faceted [110] is favourable due to much lower surface energy increase of the system than gold plating on [111] faces and suppose to retain the triangular shape of the initial SNPr. But absence of preformed gold nanoparticles causes an inefficient gold plating on [110] compared to etching process and leads to undefined gold triangular structures in absence of ascorbic acid. Disproportionation reaction between Au^{3+} and Ag^0 results transformation of three silver atoms from SNPr surface to solubilise three silver atoms as Ag$^+$ by only one gold ion (Au^{3+}) and leads all Ag atoms completely displaced by the Au^{3+} ions and form smaller Au nanoparticles with etching generated free PVP surfactant molecules. To confirm this, we have performed the elemental mapping using EDX and Figure 4a-c shows that the nanostructure is made of only Au and there is no existence of Ag in absence of ascorbic acid. In the next step we have added 100 µL ascorbic acid in the SNPr solution which can't reduce Ag atoms further from SNPr surface as all the silver atoms are already in the lowest reduction states and as a result added ascorbic acid molecules remain unreacted in the solution. If we check the reduction potentials of Au^{3+} ions in different oxidation states $(E_{Au^{3+}/Au^+}^0 = 1.36V, E_{Au^{3+}/Au^0}^0 = 1.5V, and E_{Au^+/Au^0}^0 = 1.83V)$, it is clear that though Au$^{3+} \rightarrow$ Au$^+$ is a favourable path compared to Au$^{3+} \rightarrow$ Au^0, unfavourable reduction potential for Au$^+ \rightarrow$ Au^0 force Au^{3+} ions directly reduce to Au^0 (neutral gold atoms) which is necessary for subsequent gold plating. Once we add HAuCl$_4$ to the SNPr-ascorbic acid mixture, some of the Au^{3+} ions turn immediately to Au^0 state by ascorbic acid reduction and may form small gold nanoparticles by using same ascorbic acids as surfactants[35] and rest of the gold ions remain as Au^{3+} in the system. Au^0 has strong deposition power where as Au^{3+} has high etching power. From the previously discussed surface free energy point of argument, gold crystallization on the [111] faces will result in a much larger energy increase of the system than gold plating on the edges [110]. Presence of 100µL (0.1M) ascorbic acid in 5mL SNPr solution is not sufficient to reduce all Au^{3+} to Au^0 and hence we can expect the extended role of both Au^{3+} and Au^0 in the etching cum plating process. Since the presence of ascorbic acid force the system to adopt two competing process of

gold plating and etching, gold plating on [110] faces forced the Au^{3+} ions to start the etching process from [111] facets. This is exactly the case we have observed in presence of 100μL of 0.1M ascorbic acid. Figure 3b shows the effect of $HAuCl_4$ on SNPrs in presence of ascorbic acid where SNPrs transformed into gold plated (~2.5nm) half etched BiMNRs. This is obvious from the elemental mapping of these structures which reveals the existence of Ag as well as Au (Figure 4d-f). In the final step, we have used 300 μL of ascorbic acid and in this case 3 times more amounts of Au^{3+} ions were turned into Au^0 state by ascorbic acid reduction and 3 times less amount of gold ions remain as Au^{3+}. As a result, the rate of etching should reduce 3 times where as the extent of

gold plating increases (as observed from relative thickness, thickness of structured gold wall changes from 2.5nm to 7.6nm in presence of 300μL ascorbic acid) threefold due to three fold increment of Au^0 atoms which are responsible for effective gold plating. Moreover, favourable gold plating on [110] faces increases the free energy of [111] facets and destabilizing the same facets to help faster complete etching and results Au nanoring structures. Elemental mapping as depicted in Figure 4g-i clearly shows that the resulting GNRs are composed only of Au with three times thick (7.6 nm) gold walls by using SNPr as the template.
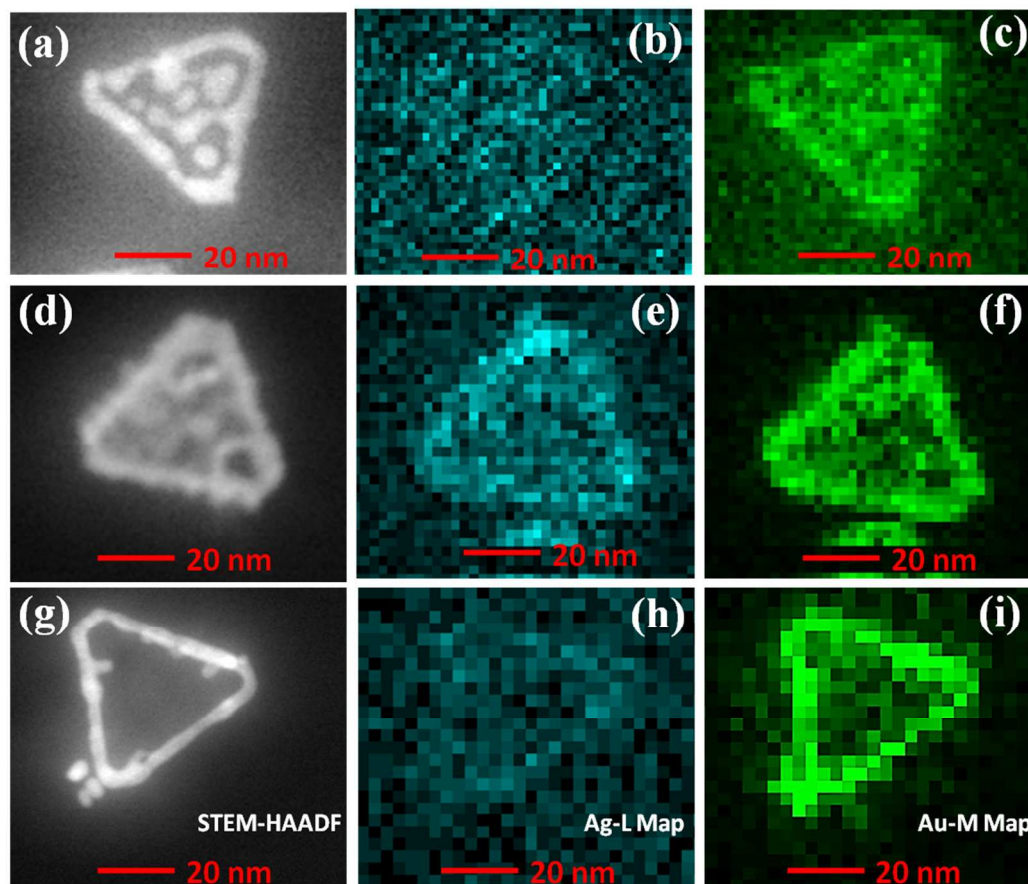

Fig. 4 STEM-HAADF-EDX images of structures produced by the addition of (a-c) 0μL of ascorbic acid, (d-f) 100 μL of ascorbic acid, and (g-i) 300 μL of ascorbic acid.
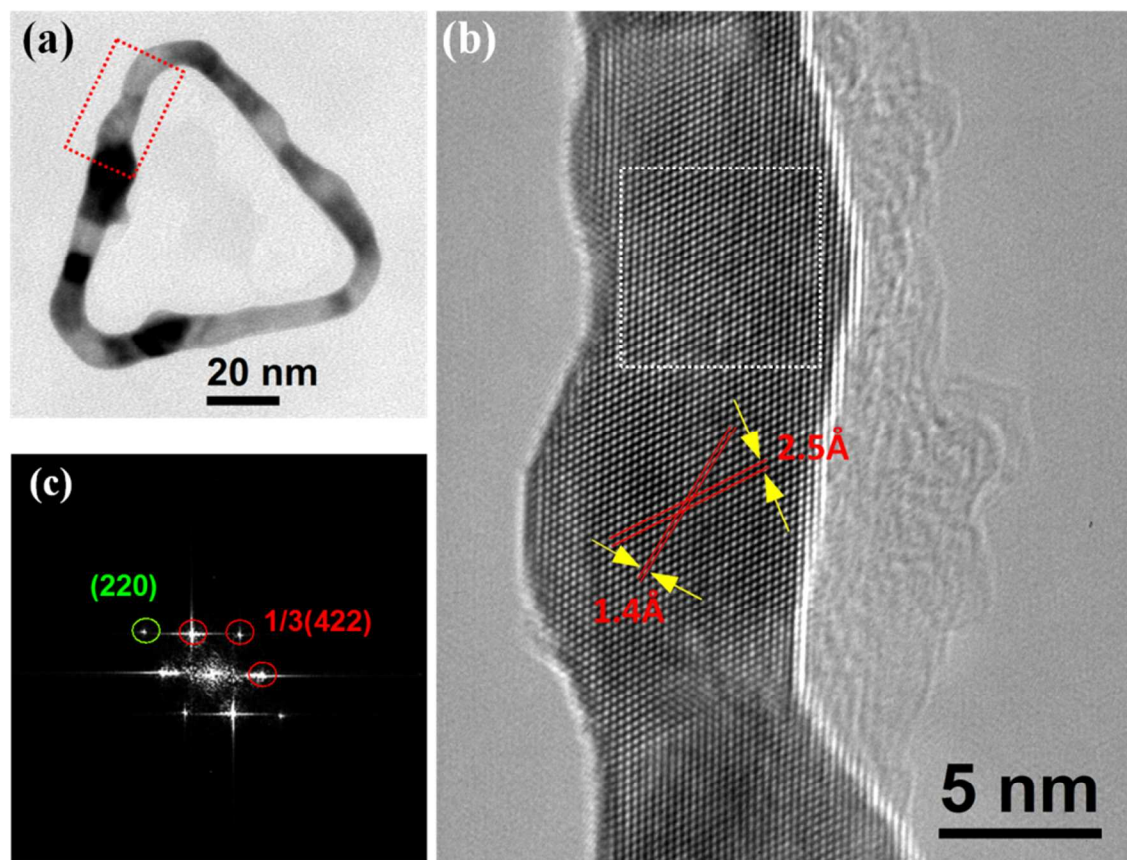
ARTICLE TYPE

Fig. 5(a) Bright-field TEM image of a triangular Au nanoring. (b) HRTEM image taken from part of the nanoring indicated in (a). (c) FFT pattern obtained from dotted box in HRTEM image

5 Figure 5a shows the bright-field TEM image of an Au ring with edge length 85 nm. Analyzing the HRTEM image and FFT of Au nanoring, we observed that single crystalline silver (as template) led to the formation of gold nanorings with single crystalline walls. The HRTEM image shown in Figure 5b from a region 10 marked by dotted box in Figure 5a reveals lattice fringes with fringe spacing 2.5 Å. This lattice spacing can be assigned to 3×{422} lattice planes for crystalline fcc gold. FFT obtained from HRTEM image of individual nanorings clearly indicate that they are single crystals, with {111} planner surfaces. The FFT 15 pattern and HRTEM image indicated that these Au nanorings had a symmetry similar to silver template, with their faces being {111} planes. On the basis of these observations, it is understood that there exits an epitaxial relationship between the Au nanorings and silver templates. Younan Xia and co-workers also 20 reported the existence of epitaxial relationship between silver templates and the gold shell structures on the basis of their HRTEM and electron diffraction studies.[24]
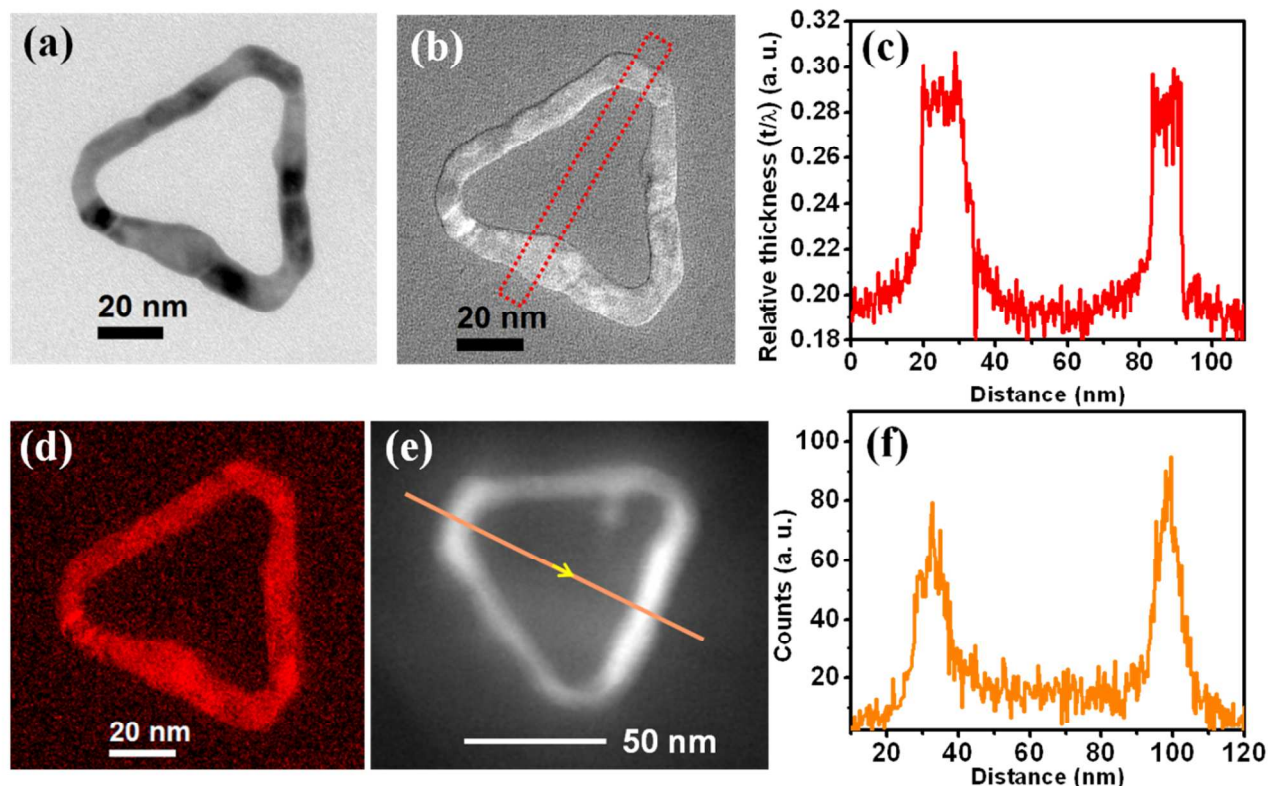
Journal Name

ARTICLE TYPE

Fig. 6 (a) Bright-field TEM image of Au-ring. (b) Relative thickness map using EFTEM showing the flattop morphology of Au nanoring. (c) Line profile shows relative thickness. (d) Elemental map of the ring using EFTEM imaging with Au-N edge. (e) STEM-HAADF imaging of Au ring. (f) Drift corrected EDX line profile of Au ring using Au-M energy.

We have analyzed the thickness and the composition of the triangular Au nanorings as presented in Figure 6. Figure 6a is the bright-field TEM image of a nanoring taken in this study. Figure 6b displays the relative thickness map of an Au nanoring.[3, 36] Figure 6c depicts the line profile of relative thickness of the Au ring along the dotted box indicated in Figure 6b. Relative thickness here again shows 2D structure with flat-top morphology. From this line profile we obtained the relative thickness of the Au ring is about 0.08 which provides the absolute thickness as 9 nm since the inelastic mean free path of Au at 300KeV energy is about 120 nm.[33] Compositional analysis of the Au ring have been performed by EFTEM imaging using Au-N edge (83 eV) with slit width 8 eV is shown in Figure 6d. EFTEM image indicates the ring is made of gold only. STEM-HAADF image and drift corrected EDX line profile of the Au ring are presented in Figure 6e and Figure 6f, respectively. Line profile using Au-M energy was carried out on one individual Au ring. Larger counts at the walls of the rings provide the further confirmation that Au rings are made of gold.

Characterization of Au-Core — Ag-Shell Nanorings

We have successfully produced bimetallic Au core – Ag shell ring structures using well-defined monometallic Au rings as template using ascorbic acid. Figure 7a shows the bright-field TEM image of a typical core-shell triangular bimetallic nanoring having triangular void space. STEM-HAADF image of the same ring is shown in Figure 7b. The core is brighter compared to the outside shell, which indicates the presence of a high-Z element at the core and a low-Z element at the shell, and in this case, it is gold and silver, respectively.
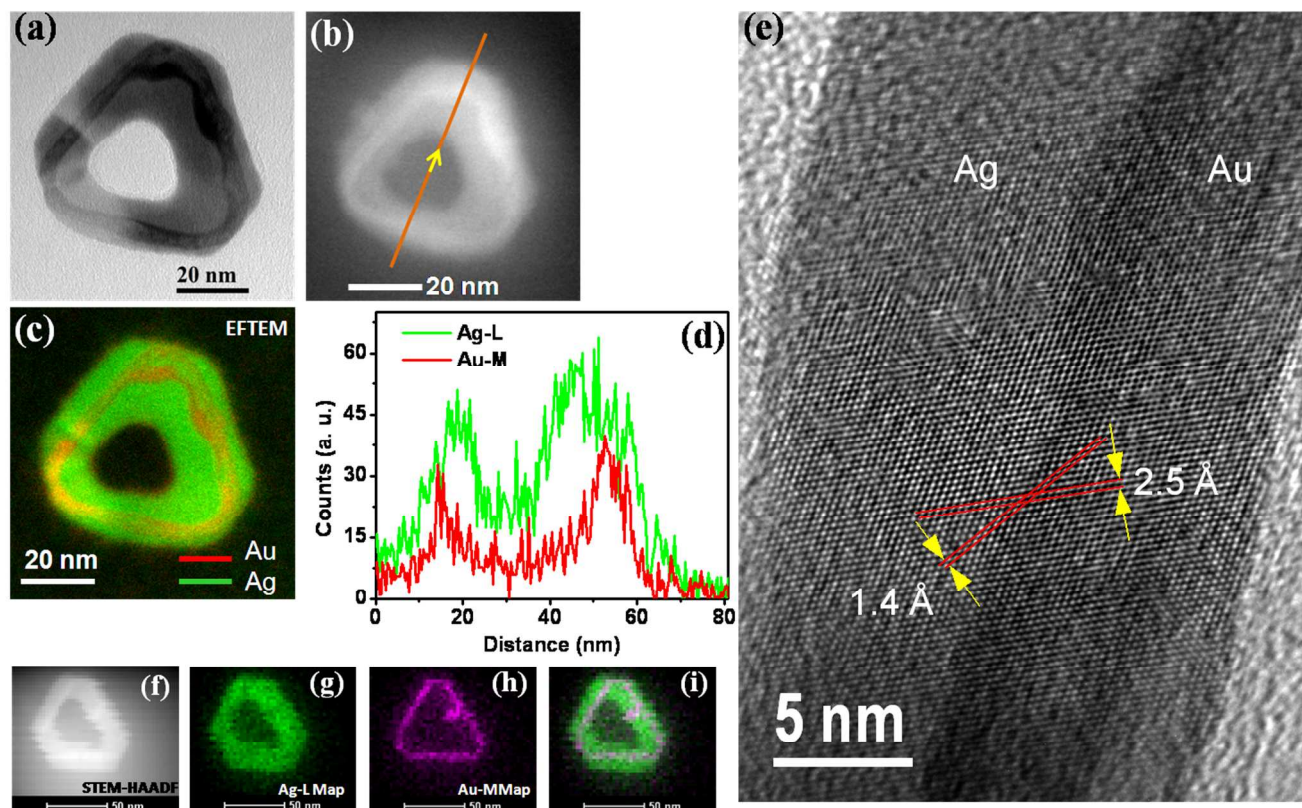
ARTICLE TYPE

Fig. 7(a) Bright-field TEM image of triangular Au-Ag ring. (b) STEM-HAADF imaging of the same Au-Ag ring. (c) Elemental mapping using EFTEM imaging with Au-N and Ag-M edge. (d) Drift corrected EDX line profile using Au-M and Ag-L energy. (e) HRTEM image taken from part of the Au-Ag nanoring. (f) STEM-HAADF image of a Au core Ag shell ring. (g), (h), (i) are the Ag-L map, Au-M map and Ag-L, Au-M combined map respectively.

Elemental mapping (Figure 7c) of the core-shell nanoring using Au-N (83 eV) and Ag-M (367 eV) edges following the EFTEM imaging technique confirms the core is made of gold and the shell is made of silver. To confirm further the composition of the core−shell structure, we have performed elemental mapping using the STEM-HAADF-EDX technique using Au-M and Ag-L energies. Figure 7d shows the EDX line profile along the line indicated in Figure 7b which reveals that the core is made of Au (red line) and the surrounding shell is made of Ag (green line). The HRTEM image (Figure 7e), taken from a portion of that core-shell nanoring shows a clear Z-contrast difference due to gold and silver. The measured lattice spacing (d-spacing) for both the Au-core and the Ag-shell is 2.5 Å and it is also to be noted that there is no lattice imperfection or mismatch at the interfaces between the Au regions and Ag regions. The HRTEM image of bimetallic core-shell nanoring is exactly similar to that of monometallic Au nanoring. From these observations we can conclude that the silver shells were overgrown epitaxially on triangular Au nanorings in both inner and outer directions to create core-shell nanorings. We have also carried out STEM-HAADF-EDX elemental mapping of an Au-Ag nanoring. Figure

7f shows the STEM-HAADF image. Figure 7g and 7h represent the Ag-L and Au-M images respectively. In the combined image shown in figure 7i it is clear that core is made of gold and shell is made of silver.

We have also carried out the relative thickness measurement of the same Au core Ag shell nanoring which is shown in figure 8a. Figure 8b shows the line profile of the relative thickness map from which relative thickness can be calculated as 0.09. Since the mean free path of Au at 300KeV energy is about 120 nm, the absolute thickness of the Au-Ag nanoring can be measured about 11 nm where as wall width is about 20 nm. Atomic force microscopy (AFM) measurement of similar size core-shell nanoring and corresponding line profile is presented in figure 8c and d, respectively. AFM measurement matches well with relative thickness measurement. Gold ring is covered by silver as evident from EDX elemental mapping.
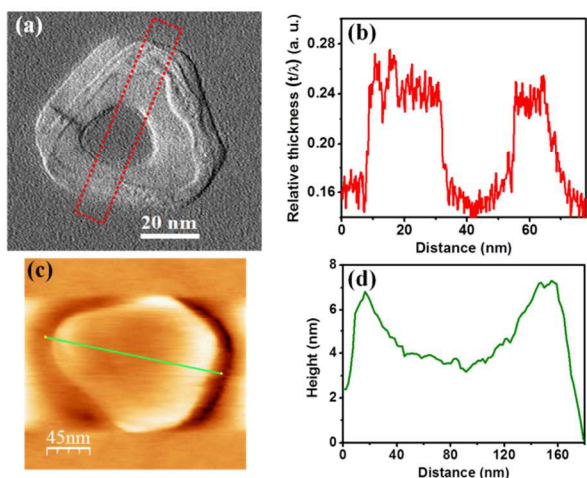
Fig. 8(a) Relative thickness map using EFTEM showing the flat-top morphology of Au-Ag nanoring. (b) Line profile shows relative thickness of the Au-Ag nanoring along the dotted box indicated in (a). (c) AFM image of a core-shell nanoring. (d) Line profile shows relative height of the nanoring along the line indicated in (c).

Conclusions

We have conducted a systematic study towards the fabrication of bimetallic nanoring growth at room temperature using ascorbic acid. We have addressed the role of ascorbic acid in this synthesis. Detailed SAED pattern and HRTEM image investigations explore that single crystalline Ag templates led to the formation of continuous Au ring in presence of ascorbic acid which finally lead to Au-Ag nanorings with single crystalline walls and there exits an epitaxial relationship in the core-shell structures. We have used STEM-HAADF, EDX and EFTEM extensively in this study for compositional analysis and to confirm 2D morphology. There are several aspects to this method. First, we can easily tune the diameter of the nanorings by altering the size of the SNPr template. Second, one can make these structures in relatively high yield with reasonable stability. Finally, these features enable us to tune the LSPR peak wavelengths of the nanorings over a wide range which may provide the opportunity to prepare the plasmonic sensors of broad variety.

Notes and references

Saha Institute of Nuclear Physics, 1/AF Bidhannagar, Kolkata-700 064, India. E-mail: biswarup.satpati@saha.ac.in

† Electronic Supplementary Information (ESI) available: [details of any supplementary information available should be included here]. See DOI: 10.1039/b000000x/

1 L. Chuntonov, M. Bar-Sadan, L. Houben and G. Haran, *Nano. Lett.* 2012, **12**, 145.

2 I. Pastoriza-Santos and L. M. Liz-Marzán, *J. Mater. Chem.* 2008, **18,** 1724.

3 T. Ghosh and B. Satpati, *J. Phys. Chem. C* 2013, **117**, 10825.

4 E. Mathlowitz, J. S. Jacob, Y. S. Jong, G. P. Carino, D. E. Chickering, P. Chaturvedl, C. A. Santos, K. Vijayaraghavan, S. Montgomery, M. Bassett and C. Morrell, *Nature* 1997, **386**, 410.

5 S. W. Kim, M. Kim, W. Y. Lee and T. Hyeon, *J. Am. Chem. Soc.* 2002, **124**, 7642.

6 I. Gill and A. Ballesteros, *J. Am. Chem. Soc.* 1998, **120**, 8587.

7 A. E. Neeves and M. H. Birnboim, *J. Opt. Soc. Am. B* 1989, **6**, 787.

8 C. Liusman, S. Li, X. Chen, W. Wei, H. Zhang, G. C. Schatz, F. Boey and C. A.Mirkin, *ACS Nano* 2010,**4**, 7676.

9 S. R. Sershen, S. L. Westcott, N. J. Halas, and J. L. West, *J. Biomed. Mater. Res.* 2000, **51**, 293.

10 J. L. West and N. J. Halas, *Curr. Opin. Biotech.* 2000, **11**, 215.

11 N. Toshima, and T. Yonezawa, *New J. Chem.* 1998, **22**, 1179.

12 Y. Sun, B. Mayers and Y. Xia, *Nano Lett.* 2003, **3**, 675.

13 I. Pastoriza-Santos and L.M. Liz-Marzán, *Nano Lett.* 2002, **2**, 903.

14 S. Chen and D. L. Carroll, *Nano Lett.* 2002, **2**, 1003.

15 K.K. Caswell, C. M. Bender and C. J. Murphy, *Nano Lett.* 2003,**3**, 667.

16 N. Malikova, I. Pastoriza-Santos, M. Schierhorn, N. A. Kotov and L.M. Liz-Marzán, *Langmuir* 2002, **18**, 3694.

17 Y. Sun, B. Gates, B. Mayers and Y. Xia, *Nano Lett.* 2002, **2**, 165.

18 M. Tsuji, D. Yamaguchi, M. Matsunaga and K. Ikedo, *Cryst. Growth Des.* 2011, **11**, 1995.

19 M. Tsuji, D. Yamaguchi, M. Matsunaga and M. J. Alam, *Cryst. Growth Des.* 2010, **10**, 5129.

20 M. Tsuji, N. Miyamae, S. Lim, K. Kimura, X. Zhang, S. Hikino and M. Nishio, *Cryst. Growth Des.* 2006, **6**, 1801.

21 X. Ye, L. Jin, H. Caglayan, J. Chen, G. Xing, C. Zheng, V. Doan-Nguyen, Y. Kang, N. Engheta, C. R. Kagan and C. B. Murray, *ACS Nano* 2012, **6**, 2804.

22 Michelle L. Personick and C. A. Mirkin, *J. Am. Chem. Soc.* 2013, **135**, 18238.

23 C. Lofton and W. Sigmund, *Adv. Funct. Mater.* 2005, **15**, 1197.

24 Y. Sun and Y. Xia, *Adv. Mater.* 2003, **15**, 695.

25 Y. Sun, B. T. Mayers and Y. Xia, *Nano Lett.* 2002, **2**, 481.

26 L. P. Jiang, S. Xu, J. M. Zhu, J. R. Zhang, J. J. Zhu and H. Y. Chen, *Inorg. Chem.* 2004, **43**, 5877.

27 G. S. Metraux, Y. C. Cao, R. Jin and C. A. Mirkin, *Nano Lett.* 2003,**3**, 519.

28 G. S. Métraux and C. A. Mirkin, *Adv. Mater.* 2005, **17**, 412.

29 B. Rodríguez-González, A. Burrows, M. Watanabe, C. J. Kiely and L. M. Liz-Marzán *J. Mater. Chem.* 2005, **15**, 1755.

30 S. A. Maier, in *Plasmonics: Fundamentals and Applications*, Springer, New York, 2007**,** ch. 5, pp. 65-88.

31 A. Henglein, Chem. Phys. Lett. 1989, **154**, 473.

32 J. Belloni, M. Mostafavi, H. Remita, J. L. Marignier and M. O. Delcourt, *New J. Chem.* 1998, **22**, 1239.

33 R.F. Egerton, in *Electron Energy-Loss Spectroscopy in the Electron Microscope*, Springer, New York, 3rd edn., 2011, ch. 5, pp. 419-422.Z.

34 L. Wang, *J. Phys. Chem. B*. 2000,**104**, 1153.

35 D. Senapati, S. SR Dasary, A. K. Singh, T. Senapati, H. Yu, P. C. Ray, *Chem. A. Eur. J.* 2011,**17**, 8445.

36 H. R. Zhang, R. F. Egerton and M. Malac, *Micron* 2012, **43**, 8.

Table of Contents:

We demonstrate the role of ascorbic acid in synthesizing bimetallic core shell nanorings at room temperature using Galvanic replacement reaction followed by epitaxial growth. The undefined gold triangular structures formed in absence of ascorbic acid where as continuous gold rings formed using ascorbic acid.